Modeling the radio echo reflections inside the ice sheet at Summit, Greenland

W. D. Miners and E. W. Wolff
British Antarctic Survey, Cambridge, UK

J. C. Moore
Arctic Centre, University of Lapland, Rovaniemi, Finland

R. Jacobel
Department of Physics, St. Olaf College, Northfield, Minnesota, USA

L. Hempel
Institut für Geophysik, Forschungsstelle für Physikalische Glaziologie, Universität Münster, Münster, Germany

Received 18 April 2001; revised 13 December 2001; accepted 18 December 2001; published 24 August 2002.

[1] Radio echo surveys to determine the thickness of ice sheets often record reflections from inside the ice. To increase our understanding of these internal reflections, we have used synthetic seismogram techniques from early seismic modeling to construct two models. Both models were one-dimensional; the first considered only primary reflections, while the second included both primary and multiple reflections. The inputs to both models were a radio pulse and data from the Greenland Ice Core Project (GRIP) core of length 3028 m. The ice core data consisted of a profile of the high-frequency conductivity, calculated from dielectric profile (DEP) measurements, and a smooth profile of the real permittivity. The models produced synthetic radargrams which are the energy reflected from conductivity variations as a function of the two-way travel time. Both models gave similar results, indicating that multiples do not alter the travel time of the reflections, i.e., no O'Doherty-Anstey effect at our time resolution. One of the results was then processed to simulate the reflected energy passing through the receiver circuit of a radio echo system and then compared with a recorded trace. The processed result contained many of the larger reflections recorded below about 500 m, including nearly all the features from depths greater than 1500 m, in particular, several interstadial events in the Wisconsin age ice. Since high-frequency conductivity variations are dominated by chemical changes which are caused by deposition on the surface of the ice sheet, it is possible to conclude that the reflections deep inside the Greenland ice sheet can be treated as isochrons. *INDEX TERMS:* 0689 Electromagnetics: Wave propagation (4275); 1827 Hydrology: Glaciology (1863); 1863 Hydrology: Snow and ice (1827); 3210 Mathematical Geophysics: Modeling; 6964 Radio Science: Radio wave propagation; *KEYWORDS:* GRIP, radio echo, DEP, conductivity, radargram, seismogram

1. Introduction

[2] *Robin et al.* [1969] hypothesized that deep internal reflections in an ice sheet could be treated as surfaces of constant age (isochrons). If the hypothesis is true, it would allow the findings at any given drill site to be extrapolated over a region covered by a radio echo (radar) survey that passed through the drill site. It would also mean that the spacing and divergence of internal reflections seen in surveys of ice sheets would provide additional information for workers modeling the flow of the ice [*Whillans*, 1976; *Paterson*, 1994].

0148-0227/02/2001JB000535$09.00

[3] To establish that an internal reflection traced over a large area is an isochron, it is first necessary to date the reflection at a single location. At a single location an ice core is necessary to establish an age-depth relation. If a feature in the ice core can be dated and correlated with a reflection, then both can be given the same date. There have been many comparisons of profiles of ice core properties against radio echo profiles collected at the same site [e.g., *Clough*, 1977; *Ackley and Keliher*, 1979; *Hammer*, 1980; *Millar*, 1981b, 1982; *Nishio and Ohmae*, 1985; *Yoshida et al.*, 1987; *Blindow*, 1994a]. The problems of such comparisons are discussed by *Gudmandsen* [1975].

[4] A better method to correlate a feature in an ice core to a reflection is by a model whose inputs are the ice core properties and a radio pulse, and whose output is a reflec-

tion profile. If the model is one-dimensional, then any reflection in the output can be related to the core properties at a single depth. Such models were used widely and successfully in early investigations of seismic waves to produce synthetic seismograms and develop an understanding of the causes of the reflections [*Peterson et al.*, 1955; *Dennison*, 1960]. We use one-dimensional models in this paper to produce synthetic radargrams [*Moore*, 1988b].

[5] A phenomenon of one-dimensional seismic models which include multiple reflections is that very short-delay "peg-leg" multiple paths cause a slightly delayed signal to become stronger than the direct transmitted signal. This effect can lead to an alteration in the arrival times of reflections and is called the O'Doherty-Anstey effect [*O'Doherty and Anstey*, 1971]. This can lead to the prediction not matching the recorded reflections. In order to see if this happened in our modeling we constructed two models, one of which considered only primary reflections, while the other considered both primary and multiple reflections. The outputs from the two models are compared with each other in this paper, allowing a conclusion to be reached on the importance of this effect. After this first comparison we then compare the output of one of the models with radio echo data. This enables us to arrive at some conclusions on the origin of the reflectors deep inside the ice sheet, and whether they can be treated as isochrons.

2. Background

2.1. Internal Reflections

[6] Weak, stratified internal reflections from deep inside an ice sheet were first noticed in 1964 during a traverse of northwest Greenland by a group from the Scott Polar Research Institute [*Bailey et al.*, 1964]. When a single pulse was transmitted into the ice there was a continuous energy return in the first few microseconds. This was expected, and attributed to the many density variations in the firn near the surface. However, unexpected weak reflections were recorded after the end of the continuous signal, but before the arrival of the bedrock reflection [*Robin et al.*, 1969]. The majority of the traverse was surveyed using a form of display called a "Z scope," where the returning energy is differentiated, and each trace is plotted against time adjacent to the previous trace. On such displays these weak reflections had some continuity parallel to the surface and behaved as if originating from specular, polished reflectors lying parallel to the surface [*Evans*, 1966]. Weak internal reflections are now noticed routinely with a variety of radar systems in Greenland, Antarctica and other polar regions [*Bogorodsky et al.*, 1985].

2.2. Understanding Internal Reflections

[7] The development of an understanding of the cause of internal reflections can be related to the growing knowledge of the factors influencing the electrical properties of ice. Early studies revealed that the relative real permittivity (ε'_r) of ice had a plateau in the radio frequency region ($\varepsilon'_{r\infty}$), often called the high-frequency value, and that this value could be related to density. This led to the first hypothesis that each internal reflection was caused by the existence of a single discrete layer of ice with a higher density (and hence a higher $\varepsilon'_{r\infty}$) than the ice above and below [*Robin et al.*, 1969]. Subsequent experiments with polar ice and firn confirmed the hypothesis, and went on to consider how monochromatic waves traveling through ice sheets would be reflected from such layers [*Paren and Robin*, 1975; *Paren*, 1981].

[8] An improved model considered the reflection strength from a statistical variation of $\varepsilon'_{r\infty}$ with depth [*Harrison*, 1973]. Harrison concluded that in those parts of the record where no single strong reflection dominated, the echo received at the surface consisted of the interference between many weak reflections from small changes in $\varepsilon'_{r\infty}$. Such a model agrees with the observed behavior of the reflections on radio echo profiles when either the duration of the transmitted pulse is altered [*Robin et al.*, 1969; *Harrison*, 1972; *Gudmandsen*, 1976; *Jacobel et al.*, 1993], or the frequency is changed [*Millar*, 1981a].

[9] Deep inside ice sheets, densification reduces the variation in $\varepsilon'_{r\infty}$ and variation of other properties becomes the dominant mechanism causing reflections. The calculated depth at which density variation is no longer dominant has become shallower as research has progressed: 1500 m [*Paren and Robin*, 1975], 1000 m [*Clough*, 1977; *Robin et al.*, 1969], 500 m [*Millar*, 1981b], 250 m [*Moore*, 1988a]. Recent work by *Fujita et al.* [1999], measuring at two frequencies in Antarctica, has put the transition just below 1000 m. However, the densification for any particular site will vary with the latitude and local climate.

[10] Ice has a small conductivity (σ) which, similar to ε'_r, has a plateau in the radio frequency region (σ_∞). It has long been known that the conductivity can be altered by adding chemicals to the water prior to freezing the sample [e.g., *Camplin and Glen*, 1973]. However, polar ice was thought to be relatively free of chemicals, and it was only as a result of later measurements that the conductivity of polar ice was shown to vary with depth. This led to the suggestion that the downward-propagating electromagnetic pulse could be reflecting from variations in the conductivity. An early paper considering this phenomenon hypothesized that either step changes in conductivity or layers with a larger conductivity, were responsible for the internal reflections [*Paren and Robin*, 1975].

[11] Another possible cause of internal reflections is anisotropy of ice crystals. In a sample of polar ice there are many single crystals each orientated in a different direction, possibly with one or more preferred orientations giving the sample a fabric. *Hargreaves* [1977, 1978] showed how the real part of the permittivity tensor could be calculated from the fabric. This led to a series of papers which have suggested that the variations in the real part of the permittivity tensor could be causing reflections [*Clough*, 1977; *Fujita and Mae*, 1994].

[12] As more measurements were made on ice cores, authors were able to make better estimates of the relative importance of the different mechanisms in producing reflections [*Ackley and Keliher*, 1979]. The factors controlling where the real permittivity and conductivity of polar ice plateau in the radio-frequency region have recently been summarized [*Miners*, 1998; *Wolff*, 2000]. The real part of the permittivity tensor is most likely to alter abruptly due to a change in the porosity or fabric of the ice. The conductivity tensor is most likely to alter abruptly due to changes in the impurity content or porosity.

[13] Near the surface, density variations (for example, in firn with occasional icy melt layers), will be the dominant cause of reflections. Deeper in the ice, where density variations are very small, changes in fabric can change the permittivity by a maximum of about 1% [*Matsuoka et al.*, 1997a], while changes in impurity content can alter the conductivity by threefold or more. Which factor is more important depends on the relative magnitude of fabric and conductivity variations, on the ice temperature, and on the frequency of the radar [*Fujita et al.*, 2000]. For central Antarctica, *Fujita et al.* [1999] have shown that fabric variations could play an important role. The balance is shifted strongly toward conductivity being more important at warmer sites, such as those in central Greenland. At Summit, there are large conductivity contrasts both in volcanic eruptions and between warm and cold phases of Dansgaard-Oeschger cycles. There is also no evidence [*Thorsteinsson et al.*, 1997] for the persistent variations (of 30% or more) with depth of crystal orientation fabrics that would be needed [*Fujita et al.*, 2000] to alter the real permittivity enough to play a significant role. It is therefore likely, that the effect of conductivity dominates, particularly at the frequency of 60 MHz considered in this paper.

2.3. Synthetic Radargrams

[14] Synthetic radargrams are produced using models that convolve idealized radar pulses with reflectivity coefficients derived from measurements on the ice core. All the models described here are one-dimensional, and treat the electromagnetic pulse from the antenna as propagating downward perpendicular to a horizontally stratified ice sheet. The ice properties in each layer are considered to be isotropic and only the high-frequency values $\varepsilon'_{r\infty}$ and σ_∞ are used in each layer. The models differ only in whether they include a frequency dependence in the reflection coefficient, multiple reflections or absorption.

[15] The first published synthetic radargram for radio echo sounding of ice was by *Moore* [1988b]. His model considered frequency-independent primary reflections without absorption and produced a predicted power reflection profile. Moore's data came from a 133 m long ice core recovered from Dolleman Island, Antarctica. The $\varepsilon'_{r\infty}$ was assumed to be constant with depth, and the σ_∞ profile was calculated from dielectric profile measurements (DEP) with a resolution of 5 cm [*Moore and Paren*, 1987]. However, no radar data were available for comparison with his prediction.

[16] More recently, a 215 m long ice core was recovered from the Filchner Ronne ice shelf. On this core meter-spaced measurements of density were used to calculate the $\varepsilon'_{r\infty}$ profile and the electrolytic conductivity of melted samples, with a mean sample spacing of 0.6 m (H. Oerter, unpublished data, 2001) were used to calculate the σ_∞ profile. At this site a radio echo survey was available, and two authors have undertaken modeling. The first, *Stock* [1993], included frequency-dependent reflection coefficients, multiples and absorption in his model. His modeling obtained a fairly close match to the decay of reflected power with time and was also successful in matching the phase and amplitude of the reflection from the meteoric-marine ice boundary. The second, *Blindow* [1994b], considered frequency-independent primary reflections without multiples or absorption, and was equally successful.

[17] Blindow's model was next used on the 181 m long Thyssenhöhe ice core from near the southern summit of Berkner Island, Antarctica. The properties of this ice core were available at a finer depth resolution, having been measured at centimeter resolution using gamma ray attenuation to calculate the $\varepsilon'_{r\infty}$ profile [*Gerland et al.*, 1999] and by DEP to calculate the σ_∞ profile [*Miners and Mulvaney*, 1995]. This modeling tried, with limited success, to match the phases and amplitudes of the internal reflections in the first 100 m [*Miners et al.*, 1997].

[18] The Thyssenhöhe ice core data were then used in another study. In it four one-dimensional models were developed, one of which was a finite difference time domain model, and two of which were similar to the models described in Appendix A. The predictions from all four models matched. However, there was no success in obtaining a match between the model results and the radio echo data [*Miners*, 1998]. The lack of success may have been due to many reasons, including the possibility that a one-dimensional model is not adequate for modeling shallow reflections in the 181 m long Thyssenhöhe ice core. However, as electromagnetic waves entering an ice sheet at angles other than vertical are refracted toward the vertical as they travel down [*Rees and Donovan*, 1992], a one-dimensional model is more representative for deeper reflections in the 3028 m long Greenland Ice Core Project (GRIP) ice core now under consideration.

3. The Data

3.1. GRIP

[19] GRIP, which involved eight European nations, drilled at 72°34.5′N, 37°38.5′W, the summit of the Greenland ice sheet. Drilling started in the summer of 1989 and continued over the next three summers. On 12 July 1992, drilling stopped at a depth of 3028.65 m when the drill had penetrated 6 m of debris-laden basal ice. The GRIP drill hole did not deviate more than 3° from the vertical [*Johnsen et al.*, 1994] and less than 1 m of core was lost in the drilling process [*Dansgaard et al.*, 1993].

3.2. Relative Real Permittivity Profile Inside the Ice Sheet

[20] The variation of $\varepsilon'_{r\infty}$ with depth inside the ice sheet will determine the speed of the electromagnetic wave and the time interval between a pulse entering the ice sheet and the return of its reflection to the surface, the two-way travel time (t_{twtt}). The DEP measurement of permittivity has a poor accuracy, so errors in $\varepsilon'_{r\infty}$ would generate false reflections. Therefore, it is better to calculate $\varepsilon'_{r\infty}$ from the density (ρ, kg m^{-3}) of the ice core, using, for example, a cubic equation derived from the Looyenga equation for dielectric mixtures [*Paren*, 1970; *Glen and Paren*, 1975]. Assuming solid ice has $\varepsilon'_{r\infty} = 3.17$ and $\rho = 917$ kg m^{-3}, then

$$\varepsilon'_{r\infty} = \left(1 + 0.51 \times 10^{-3}\ \rho\right)^3. \quad (1)$$

There are other possible equations such as an empirically derived quadratic given by *Kovacs et al.* [1995]. It has been

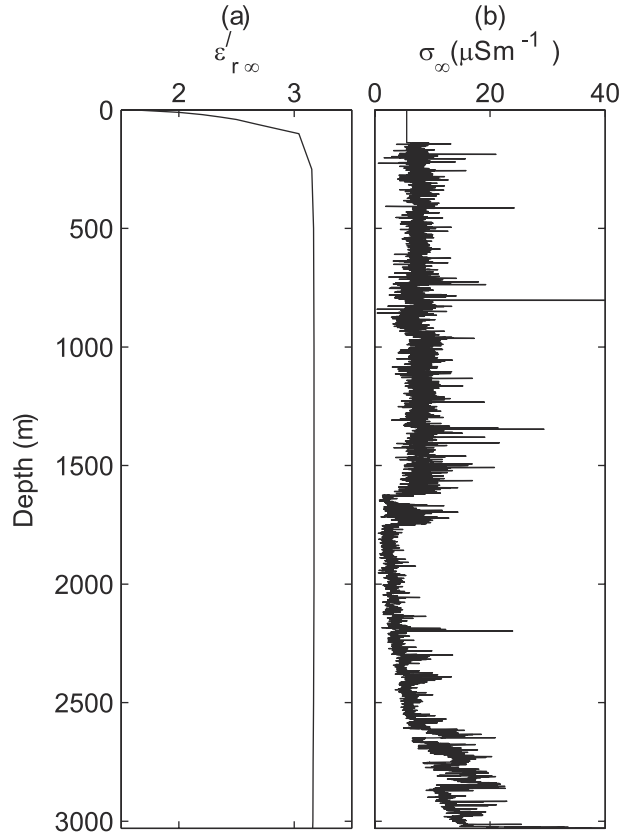

Figure 1. Ice core properties as functions of depth. (a) The high-frequency relative real permittivity, determined from a combination of density measurements at Site A and GISP2. (b) The high-frequency conductivity for the ice sheet at GRIP, determined from DEP measurements on the surface then altered to reflect values at ice sheet temperature.

shown, however, that there is little to distinguish between the many possible equations relating density and $\varepsilon'_{r\infty}$ [*Stiles and Ulaby*, 1981; *Sihvola et al.*, 1985; *Sihvola and Lindell*, 1992].

[21] Unfortunately, no weighing of the core sections was done at the GRIP drill site. Therefore, for the modeling in this paper the density record used is a combination of the measurements from two sites. First, from Site A, 170 km south of GRIP [*Alley and Koci*, 1988] which has measurements from the surface to a depth of 100 m. Second, from the GISP2 site, 30 km west of GRIP [*Gow et al.*, 1997] where there are nine measurements between the depths of 250 m and 3000 m. The fifteen $\varepsilon'_{r\infty}$ values produced from the combined measurements on the two cores are spaced too far apart vertically to give any realistic modeling of reflections from permittivity variations. However, the $\varepsilon'_{r\infty}$ values are necessary in the model to give the speed of the electromagnetic wave, which will change with depth inside the ice sheet. The values used in the model are interpolated from the available measurements. The profile of $\varepsilon'_{r\infty}$ used in the modeling is shown in Figure 1a.

3.3. Conductivity Profile Inside the Ice Sheet

[22] The conductivity inside the ice sheet at GRIP is calculated from the DEP measurements on the ice core [*Moore et al.*, 1994]. In the DEP instrument used at GRIP, both electrodes were inside an earthed box with the top electrode split into 120 two centimeter wide strips. The conductance and capacitance were measured at 20 frequencies between 120 Hz and 300 kHz; σ_∞ was then calculated by fitting these values to a linearized Debye equation. The σ_∞ record has a depth resolution of 2 cm, and extends from a value centered on 148.045 m to a value centered on 3028.600 m.

[23] The conductivity of ice increases with temperature, so that the conductivity of the ice core measured by the DEP at the surface will be different from the conductivity of the sample when it was deep inside the ice sheet. Therefore, the temperature inside the DEP box was measured during the logging of each piece of core. By combining these temperature measurements with the temperature profile of the ice sheet, calculated from lowering thermistors down the borehole [*Johnsen et al.*, 1995], it was possible to calculate the in situ σ_∞ record inside the ice sheet using the published temperature dependencies of the conductivity [*Miners*, 1998].

[24] The profile of in situ σ_∞ used in the modeling is shown in Figure 1b. The decrease in conductivity at a depth of about 1600 m corresponds to the transition from the Holocene to the Pleistocene and is discussed further in section 5.2. It can also be seen how σ_∞ increases as the base of the ice sheet is approached due to warming near the bedrock.

3.4. Radio Echo Data

[25] Three radio echo systems have been used near Summit. These are discussed below but only one will be compared with the model output. The Technical University of Denmark (TUD) system was a 60 MHz airborne burst transmission system, which when attached to a digital recording system was capable of recording reflections from the bedrock and internal layers [*Skou and Sondergaard*, 1976; *Wright et al.*, 1989; *Jacobel and Hodge*, 1995]. The Forschungsstelle für Physikalische Glaziologie (FPG) at the University of Münster provided two ground-based systems: a single pulse 35 MHz system designed to image to a depth of 1000 m; the other a 35 MHz burst transmitter used to image the bedrock [*Hempel and Thyssen*, 1992].

[26] The records from the two burst transmitter systems are relevant to this paper as they record the deep internal reflections. The details of the collection parameters for the two burst pulse systems can be seen in Table 1. In Figure 2 we compare the TUD results (collected 1500 m away from the GRIP drill site) with the FPG results (collected 20 m away from the GRIP drill site). In the single traces from the TUD data (Figure 2a) and the FPG data (Figure 2d) there are differences in the number of internal reflections visible. There are two reasons for this: First, the TUD has not had automatic gain control applied to it, and second, the FPG trace has 10 ns sampling which is four times that of the TUD. Despite differences in the individual traces, the Z scope displays in Figures 2b and 2c are similar, with "quiet regions" near 23 μs, corresponding to the top of the Pleistocene, and near 32 μs, above the bedrock. These similarities are due to both systems transmitting at frequencies where the electrical properties of the ice are similar

Table 1. Properties of the Forschungsstelle für Physikalische Glaziologie (FPG) and Technical University of Denmark (TUD) Burst Pulse Radio Echo Systems

Property	FPG	TUD
Vehicle used	Sledge	Aircraft
Height of antenna above ground, m	1	370[a]
Distance to borehole, m	20	1500[b]
Vehicle speed, m s^{-1}	1	100
Transmission rate, kHz	3.5	12.5
Center frequency, MHz	35	60
Wavelength of center frequency in ice, m	4.8	2.8
Duration of transmitted pulse, ns	500–1000	250
Length of transmitted pulse in ice, m	80–160	40
Transmitted power, kW	12–16	10
Sample interval used on returning signal, ns	10	40
Number of returning traces summed together before recording	2048	512[c]
Distance of surface travel represented by each final recorded trace, m	10–30	17[c]

[a] Calculated from the return time of the surface reflection in the radar trace.
[b] TUD radar data taken from flight line N375.
[c] Each TUD trace shown in Figure 2 has also had eightfold stacking so representing the energy collected during 136 m of surface travel.

(60 MHz for TUD and 35 MHz for FPG) and also due to the uniform stratigraphy of the ice sheet in the area where both records are collected. This uniformity extends for at least a few thousand meters, a distance comparable with the depth of the ice sheet at this location. Such a stratigraphy supports the use of horizontally stratified layers in our one-dimensional models.

[27] The similarity in the Z scope displays means that we could select either burst record for comparison with the model output. We use the TUD record since its pulse is better defined than the FPG pulse and the TUD record has reflections over the entire profile from surface to bedrock.

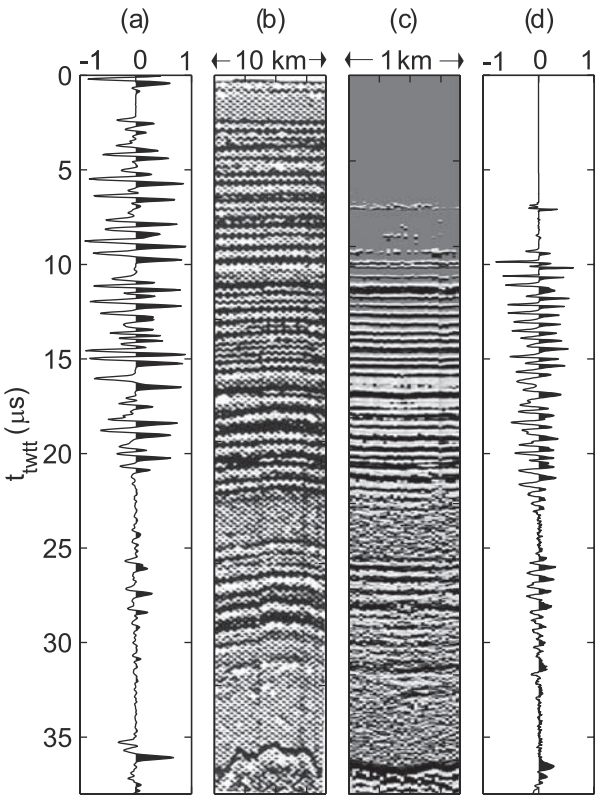

Figure 2. Radio echo data versus two-way travel time (t_{twtt}). (a) A single trace from the TUD radar. (b) A portion of the Z scope record from the TUD radar. (c) A portion of the Z scope record from the FPG radar. (d) A single trace from the FPG radar.

4. Modeling

[28] Two models will be used, both of which are one-dimensional and consider a pulse propagating perpendicular to a horizontally stratified ice sheet. A horizontally stratified ice sheet seems to be a good approximation as the slopes in the bedrock and the layers visible in the entire Z scope records are low and the echoes are largely specular.

[29] One-dimensional models cannot simulate spherical spreading of the energy as it travels out from the transmitter into the ice sheet. This means that the model result will not contain the correct decay in reflection strength as t_{twtt} increases. However, this is not a disadvantage as the recorded TUD radio echo trace does not contain the decay in reflection strength. The recorded trace has passed through several electronic filters, including a logarithmic amplifier, which have removed the information on the echo strength coming out of the ice sheet. We decided, therefore, not to compare the absolute value of the reflections in the model results and the radio echo record.

[30] The first model used in this paper considers only primary reflections: pulses that travel down to an interface, are reflected, and travel back to the surface. This model takes no account of pulses that undergo multiple reflections inside the ice sheet, nor is there any account of any losses that occur inside the ice sheet.

[31] The second model includes primary reflections, multiples and losses. The two major loss mechanisms in a one-dimensional model are absorption loss within each layer and transmission loss while crossing the interfaces between layers on the way down and up. The details of the two models are given in Appendix A.

[32] Both the models require the profiles of $\varepsilon'_{r\infty}$ and σ_∞ in the ice sheet and an estimate of the electromagnetic pulse entering the ice sheet from the radio echo system. The ice sheet is represented as a stack of 20 mm thick layers; each layer has its own values of $\varepsilon'_{r\infty}$ and σ_∞. These values were interpolated from the nearest depth ice core values [*Miners*, 1998].

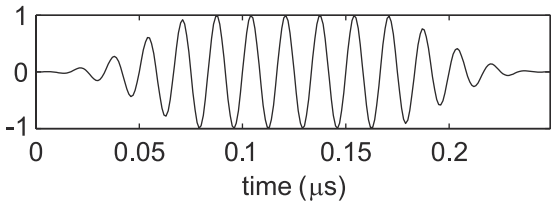

Figure 3. Pulse used to model the TUD radar; the vertical axis is in relative units.

[33] The incident pulse used in the models is a replica of the pulse transmitted by the TUD system, a 60 MHz carrier with a duration of 250 ns. An envelope is applied to the carrier which tapers off smoothly for the first and last quarter. This pulse is shown in Figure 3.

[34] It is worth briefly considering the possible changes in the results that models of higher dimensions would have produced. As discussed earlier in this section, higher dimension models would have included spherical spreading. They would also have given a more accurate representation of the impulse response at each interface between ice layers with different properties. The impulse response from a higher dimension model would have a similar initial reflection time but a longer duration tail to the reflection as the off-central axis reflections occurred at oblique angles. However, as the core data are one-dimensional, higher dimension models would require assumptions about the higher dimensional distribution of the ice sheet properties.

[35] Another possible criticism is that neither of the two models used in this paper considers the properties of the ice as tensors. This is due to the absence of tensor data for conductivity and real permittivity. A model using anisotropic properties of the ice would also require a more elaborate specification of the transmitted pulse. This omission is thought not to be important due to the small size of the anisotropy as discussed in section 2.2.

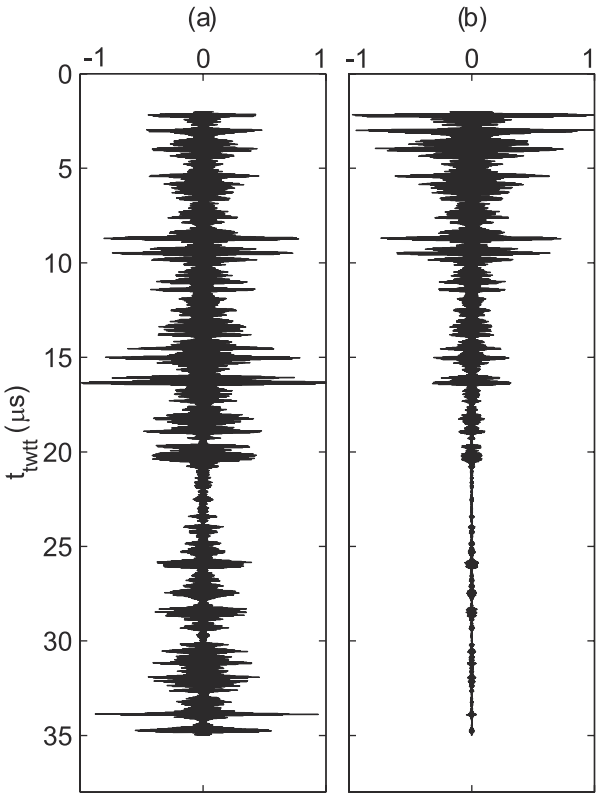

Figure 4. Comparison of the raw results from the two models. The vertical axis is the two-way travel time (t_{twtt}), and the horizontal axis is the relative strength of the electric field arriving back at the top of the ice sheet. This has been normalized for both models. (a) Model one, primary reflections only without losses or multiples. (b) Model two, primary and multiple reflections with losses.

5. Results

5.1. Comparison of Raw Results From the Two Models

[36] Figures 4a and 4b show the raw results from the two models. As described in Appendix A, these are an indication of the energy coming out of the ice sheet, before entering the receiver electronics of the radio echo system. For this reason, the main frequency content of the results is the 60 MHz frequency that was in the pulse transmitted by the TUD system. The results are only an indication of the energy that would exit the ice sheet as the models are one-dimensional and so do not include the effect of spherical spreading.

[37] The main noticeable difference in the results from models one and model two is that the inclusion of losses in model two reduces the amplitudes of the reflections from late travel times, showing the importance of conduction losses.

[38] In Figure 5 an enlarged portion of the late travel time model results are displayed, with the amplitudes normalized for the section under consideration. This figure shows that both models predict deep reflections with similar t_{twtt}. So multiple reflections and losses do not influence the travel time at the time resolutions used here, i.e., we have no evidence of an O'Doherty-Anstey effect. As the t_{twtt} of the internal reflections from both models are similar then the only consideration is whether we wish to compare the radar data with a result that has losses (model two) or a result which does not have losses (model one). We will proceed by using the result from model one as it requires fewer steps to

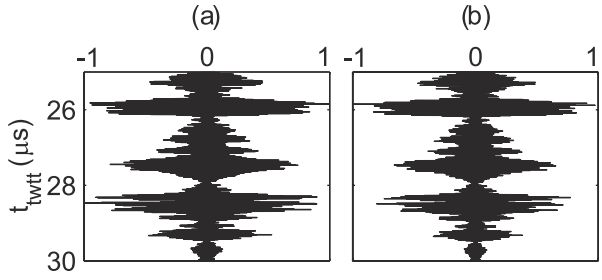

Figure 5. Comparison of the raw results from the two models for late travel times. The vertical axis is the two-way travel time (t_{twtt}), and the horizontal axis is the relative strength of the electric field arriving back at the top of the ice sheet. This has been normalized for both models. (a) Model one, primary reflections only without losses or multiples. (b) Model two, primary and multiple reflections with losses.

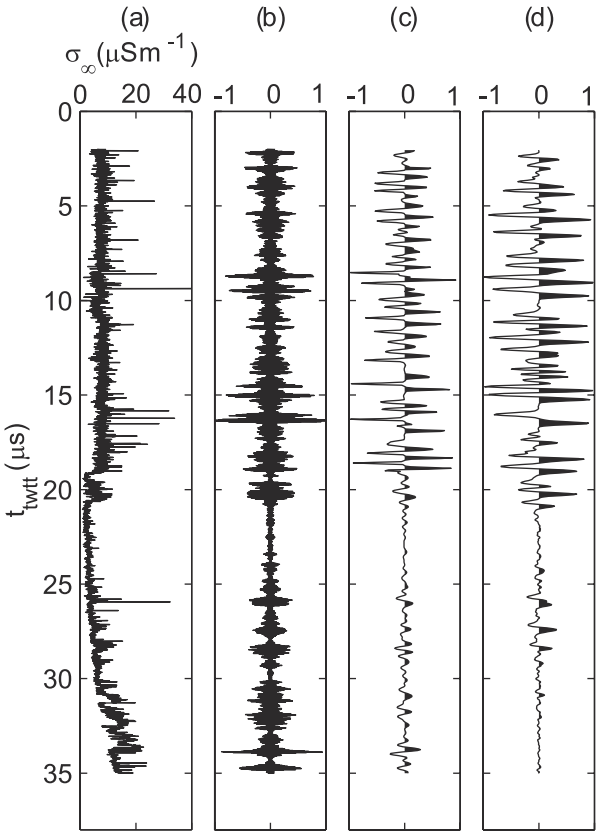

Figure 6. Comparison of the model output with the radar record. The vertical axis is the two-way travel time (t_{twtt}). (a) The σ_∞ record after conversion to a Goupillaud medium. (b) The raw result from model one. (c) The processed result from model one. (d) A single trace from the TUD record.

be comparable with the radar data, as there is no need for a t_{twtt}-dependent amplification.

5.2. Comparison of the Model Results With the Radar and the Conductivity Data

[39] The model results shown in Figures 4 and 5 are an indication of the energy coming out of the ice sheet. The recorded TUD radio echo trace looks different. This is because the energy that came out of the ice sheet passed through the receiver electronics before being written to tape. The receiver electronics, and in particular the logarithmic amplifier, removed the 60 MHz variation giving a smoothed envelope to the radio echo trace.

[40] In order to compare the model trace with the recorded radio echo trace, the model trace needs to go through a series of processing steps which try to imitate the receiver electronics. For the trace from model one these steps were: (1) apply a 4 MHz band-pass filter, (2) convert to base band (multiply by a 60 MHz carrier and then low-pass filter) and (3) take the gradient. This produces what will be called the processed model trace. It has approximately the same frequency content as the radar data. What is not known is the time lag and phase rotation that the receiver electronics would have given to the received energy. The processed model trace has been given a time shift of 0.01 μs and a phase rotation of −112° as this allows an easier comparison of the interstadial reflections, as will be discussed below.

[41] The comparison of the model to the radar is shown in Figure 6. The general form of the processed model trace (Figure 6c) and the TUD trace (Figure 6d) are similar. In the top part of the ice sheet (earlier than 20 μs), both contain many large amplitude reflections. Then, at later arrival times, both traces have fewer reflections.

[42] In the earlier part of the raw model trace (Figure 6b) a few large reflections stand out, such as those at 8 μs, 15 μs, and 17 μs. These large reflections can be related to peaks in the conductivity record (Figure 6a) and then across through the processed model trace to peaks in the TUD radar trace. This top part of the ice sheet at GRIP has been the subject of a previous comparison of radar and conductivity. *Hempel et al.* [2000] compared the results from the FPG high-resolution single pulse radar survey and electrical conductivity measurement (ECM) data from the top 800 m of the GRIP core. They found a remarkable coincidence between large ECM peaks, due to fallout of volcanic acid, and the depth of strong reflectors, suggesting that such conductivity contrasts are the dominant factor controlling internal reflections between about 180 m and 800 m depth at GRIP.

[43] At the beginning of the Holocene (a depth of 1624 m, t_{twtt} of 19 μs) there is a dip in the conductivity profile. The ice at this depth accumulated during the Younger Dryas period. This layer of lower conductivity in the ice causes few reflections in the raw model trace and lower amplitude reflections in the processed model trace. There are also lower amplitude reflections in the TUD radar trace. Immediately after this Younger Dryas period the processed model trace does not produce as large a peak as seen in the TUD radar trace. However, the longer period with fewer reflections in both model traces between 21 and 24 μs shows up clearly in the TUD radar trace.

[44] In the lower part of the ice sheet, seen in Figure 7, between a t_{twtt} of 20 and 30 μs the model results contain reflections with similar travel times and widths to the reflections seen in the radio echo data. The conductivity changes causing the reflections in this part of the ice sheet are mainly due to the alternating alkaline (stadial, cold period) and acidic (interstadial (IS), warm period) nature of the ice. Between 25 and 29 μs in the TUD trace there are a series of three reflections. Seen in more detail in Figure 7d, these are all clearly present in the raw model trace and in the increased activity of the conductivity data. The peaks in the conductivity attributed to these reflections occur during longer interstadials during the Wisconsin Glacial. They are identified as IS 8 (25.8 μs), IS 12 (27.3 μs) and IS 14 (28.3 μs). The duration of each of these events is somewhat longer than the Younger Dryas, showing that, although the events are nearly 1 km deeper in the ice, they are well detected by the TUD radar. If the electronic modification of the received signal before digitization was less extreme, it is likely that the Younger Dryas and many of the other interstadial events would be much better resolved by radar.

[45] Between 30 μs and 35 μs, seen in Figure 6, there are no major reflections in the TUD data. It has been suggested, along with other possible mechanisms, that the absence of strong reflections is due to the presence of folding near the

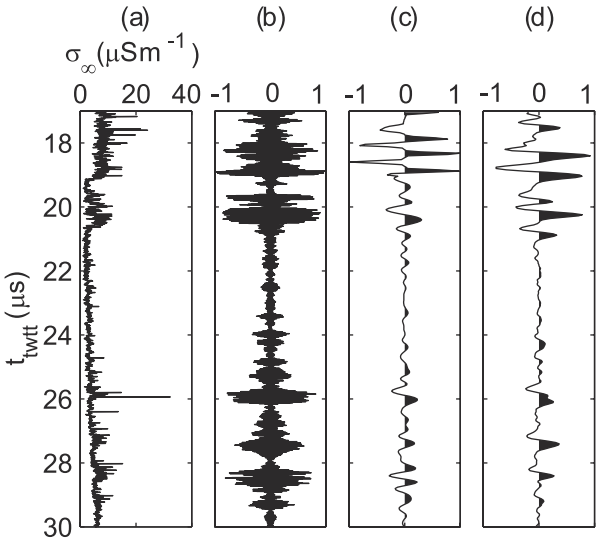

Figure 7. Comparison of the model output with the radar record for late travel times. The vertical axis is the two-way travel time (t_{twtt}). (a) The σ_∞ record after conversion to a Goupillaud medium. (b) The raw result from model one. (c) The processed result from model one. (d) A single trace from the TUD record.

base of the ice sheet [*Jacobel and Hodge*, 1995]. However, the model does predict reflections over this interval, due to assuming that boundaries seen in the ice core are continuous and flat enough to form reflections. If there is folding in the layers of ice in the base of the ice sheet, then there will not be a sufficiently continuous boundary to form a reflection. Alternatively, it may be that the amplitudes of the reflections from internal layers at this depth were too small for the TUD radar system to record.

6. Discussion and Conclusions

[46] Several properties of the ice sheet could be causing the internal reflections seen in the radio echo data. However, by using the models presented in this paper we have reproduced, at least to a first approximation, many of the features seen in the radio echo data by varying only the conductivity. In the models, the real permittivity (from density) was a smooth profile and would not have generated any reflections. Thus the only property that does vary in the models, the conductivity, is predominantly responsible for causing the reflections.

[47] Consider how the conductivity profile used in the models is derived; it is calculated from DEP measurements of capacitance and conductivity at frequencies between 20 Hz and 300 kHz. These values are then used to determine σ_∞, a value thought to be close to the true high-frequency conductivity of the ice. It has been shown in many publications [*Moore*, 1988a; *Moore et al.*, 1992a, 1992b; *Moore et al.*, 1994; *Wolff et al.*, 1995] that σ_∞ is closely correlated to the chemical impurities in the ice core. There are also models that have been produced to explain how the presence of chemical dopants can influence the number of charge carriers and hence the conductivity of the ice [*Hobbs*, 1974; *Petrenko*, 1993]. This does not preclude the possibility that the fabric may have an influence on the measured variations in σ_∞. However, the influence of fabric on σ_∞ would be limited by the anisotropy of the individual ice crystals making up the fabric of the ice in the core. For conductivity at 300 kHz, *Hobbs* [1974] gives an anisotropy of between 9% and 18%, while at 1 MHz, *Matsuoka et al.* [1997a] give a value of 20%. At higher frequencies, in the GHz range, there are detailed measurements giving a value close to 1% [*Fujita et al.*, 1993; *Matsuoka et al.*, 1997a, 1997b]. Fabric changes cannot cause more than a few percent change in the σ_∞, while it has been shown that chemical impurities can alter σ_∞ by the order of 100%.

[48] The conclusion from the modeling in this paper is that conductivity is the dominant control on radar reflections at frequencies close to 60 MHz, for at least the lower two thirds of the ice sheet at the GRIP site. Given that chemistry plays the dominant role in determining conductivity below the pore close-off depth [*Wolff*, 2000], it is therefore clear that either sharp peaks (volcanic fallout) or transitions between bands (interstadials) of increased chemical variability are the main causes of the internal reflections in Greenland. Such chemical layers will generally be spatially ubiquitous, leading to a second conclusion that the main radar reflectors are indeed isochrons that can be used to predict age-depth relationships, and as an aid to studies of ice sheet dynamics. Higher-resolution radars should enable many more isochrons to be detected, especially the long duration interstadial events in the Wisconsin age ice. The long duration of these climate events makes them certain to be well represented in the snow cover over the whole of Greenland, whereas the relatively short duration of even the most powerful volcanoes can easily be removed by wind erosion or affected by the vagaries of local deposition patterns. The greater depth of the interstadials also makes them particularly valuable in ice flow studies.

Appendix A: Description of the Models

[49] For the models used in this paper the partial differential, source-free wave equation was solved using a separation constant of $-\tilde{k}^2$, where the tilde is used to indicate a complex quantity, and a positive time exponent $e^{i\omega t}$ so

$$\tilde{k}^2 = \mu_0 \varepsilon_0 \varepsilon_r' \omega^2 - i\mu_0 \sigma \omega. \tag{A1}$$

This is similar to that of *Budden* [1985] and *Staelin et al.* [1994].

A1. The Pulse

[50] The time domain electric field of the pulse entering the ice sheet is represented in the models as a discrete time series of real numbers (the measured E field is real) sampled at an interval Δt. This series has zeros added to the end to form a length (N) to allow the use of fast Fourier transforms (i.e., N = 64, 128, 256, etc). In the frequency domain this real pulse is represented by a series of complex numbers. The frequencies are discrete and the index for the frequency used is p ($1 \leq p \leq N$). The dc value (zero hertz) is at p = 1,

and the Nyquist frequency ($f_{\mathrm{Nyq}} = 1/(2 \times \Delta t)$) is at $p = N/2 + 1$. The relationship between the index p and the frequency f are shown in

$$\begin{aligned} p &= 2 \quad 3 \quad 4 \quad \ldots \frac{N}{2} + 1 \\ f &= \frac{2f_{\mathrm{Nyq}}}{N} \frac{2 \times 2f_{\mathrm{Nyq}}}{N} \frac{3 \times 2f_{\mathrm{Nyq}}}{N} \ldots f_{\mathrm{Nyq}}. \end{aligned} \tag{A2}$$

The complex values in the frequency domain are termed the analytic function of the incident pulse ($\tilde{F}_p$). The subscript p is the index. Due to the symmetry properties of real series in the time domain, the complex values in the frequency domain beyond the Nyquist frequency ($N/2 + 2 \leq p \leq N$) are the conjugate of the values below the Nyquist ($2 \leq p \leq N/2$).

A2. Model One: Primary Reflections Without Losses

[51] The stack of layers ($1 \leq m \leq M$) each of equal thickness Δz are converted into a stack of layers ($1 \leq g \leq G$) each of equal two-way travel time Δt. This conversion is done using the non-dispersive phase velocity of the pulse in each layer and the new stack is called a *Goupillaud* [1961] medium. The pulse entering the model has 2048 samples, and as the shortest two-way travel time between the layers in the Goupillaud medium is 0.1695 ns, this means that the frequency of $p = 2$ is 2.9 MHz. This frequency is sufficiently far above the main dispersion in ice (a few kHz), to justify the use of the high-frequency values for relative real permittivity and conductivity [*Miners*, 1998].

[52] The reflected electric field at the surface starts as a discrete time series, of length $G + N$, with a time step Δt and a value of zero at each point. Each time step is the two-way travel time in a layer. The calculation considers each interface in the Goupillaud medium in turn.

[53] Between layers g and $g + 1$ the complex Fresnel (subscript F) amplitude (subscript A) reflection coefficient at each frequency index p ($\tilde{r}_{AFgg+1p}$) is calculated using

$$\tilde{r}_{AFgg+1p} = \frac{\tilde{k}_{gp} - \tilde{k}_{g+1p}}{\tilde{k}_{gp} + \tilde{k}_{g+1p}}, \tag{A3}$$

where $\tilde{k}_{gp}$ is the complex wave number in Goupillaud layer g at frequency index p. This calculation is only performed for the frequency indices p in the range: $2 \leq p \leq N/2 + 1$, where the incident pulse has an absolute magnitude in the frequency domain of greater than one thousandth of the maximum absolute amplitude. The amplitude reflection coefficient values for the other values of p are set to zero. The complex series produced by equation (A3) is multiplied with the complex analytic function of the incident pulse for the same indices ($\tilde{F}_p$). This gives the complex analytic function of the reflected pulse for the frequency indices: $2 \leq p \leq N/2 + 1$ at the interface between g and $g + 1$. It is then necessary to specify the rest of the frequency domain for the reflected pulse. The dc value ($p = 1$) is set to 0 and the complex values in the frequency domain beyond the Nyquist ($N/2 + 2 \leq p \leq N$) are determined using the symmetry properties of real series, and are the conjugate of the values below the Nyquist ($2 \leq p \leq N/2$).

[54] An inverse Fourier transform is then applied to the series to give the reflected pulse in the time domain at the interface. This is then superimposed onto the record of the electric field coming out of the ice sheet. The first value in the reflected pulse series is added to the electric field record starting at the two-way travel time (t_{twtt}) of the interface under consideration. The same procedure is repeated for all the interfaces in the Goupillaud medium, so that the reflected pulses at each interface are added to each other as they are superimposed onto the electric field record.

A3. Model Two: Primary and Multiple Reflections With Losses

[55] The first step in this model is to construct a frequency domain representation of the ground. *Trorey* [1962], when considering synthetic seismograms, discussed how the frequency domain solution for the ground contains all the multiples that last for infinite time. Transforming this (using an inverse Fourier transform) into a finite time domain would cause problems and could introduce aliasing errors. A way round this was described by *Nielsen* [1978]: assuming a periodic pulse going into the ground, it was possible to use a discrete Fourier transform as long as the period of the transmission was much longer than the arrival time of the last multiples that are of interest.

[56] This condition is ensured, in this model, by adding sufficient zeros to the end of the incident pulse so that the duration is long enough to record all the wanted reflections. As in model one the incident pulse is expressed as a discrete time series of length N which is two raised to an integer power. As the chosen sample interval was 50 ps this required $N = 2^{20}$. This meant that $p = 2$ was at a frequency of 19 kHz, and it was not until $p = 54$ that the MHz frequencies were reached. For these low frequencies calculating the reflection coefficient using $\varepsilon'_{r\infty}$ and σ_∞ would introduce an appreciable error. However, the long duration of the incident pulse meant that its analytic function was sharply peaked in the frequency domain near 60 MHz. The modeling was therefore done with a reduced section of the frequency domain, as in model one, so that the low p values could be neglected and set to zero.

[57] In this model the amplitude and phase change to each of the monochromatic waves in the reduced section of the frequency domain is considered as they travel into the ice and are reflected back. This gives the reflection coefficient of each frequency component at the top of the stack of layers. There are two algorithms that can be used for this model: propagation matrices or an impedance stack. Propagation matrices have been used by *Lanzario-Mancilla and Gomez-Trevino* [1996] and speeded up by *Choate* [1982]. Impedance stack algorithms are described by *Wait* [1958, 1996], though he uses a positive separation constant ($\tilde{\gamma}^2$) to solve the partial differential source-free wave equation. Impedance stack algorithms have been used previously in radio glaciology to consider monochromatic waves by *Ackley and Keliher* [1979] and *Moore* [1988b]. In this paper the impedance stack algorithm is used so that the complex amplitude reflection coefficient between layers 1 and 2 at each frequency index p ($\tilde{r}_{A12p}$) is given by

$$\tilde{r}_{A12\,p} = \frac{\hat{Z}_{2\,p} - Z_{1\,p}}{\hat{Z}_{2\,p} + Z_{1\,p}}, \tag{A4}$$

where Z_{1p} is the bulk impedance of the first layer at frequency index p and $\hat{Z}_{2p}$ is the input (or surface) impedance

of the second layer at frequency index p. The bulk impedance is given by

$$Z_{1p} = \sqrt{\frac{\mu_0}{\varepsilon_0 \varepsilon'_{r\infty 1} - i\frac{\sigma_{\infty 1}}{\omega_p}}} \quad , \tag{A5}$$

where ω_p is the angular frequency at frequency index p and the input impedance is given by the properties of the second and lower layers by

$$\hat{Z}_{2p} = Z_{2p} \frac{\hat{Z}_{3p} + Z_{2p} i \tan\left(\tilde{k}_{2p} \Delta z\right)}{Z_{2p} + \hat{Z}_{3p} i \tan\left(\tilde{k}_{2p} \Delta z\right)}. \tag{A6}$$

Once the reflection coefficient for the stack of layers ($\tilde{r}_{A12p}$) has been obtained for the required frequency indices in the range $2 \leq p \leq N/2 + 1$, the other frequency indices in this range are given a value of zero. This series is then multiplied with the similar range of the analytic function for the incident pulse $\tilde{F}_p$. The symmetry properties of real series are used to specify the rest of the spectrum and then an inverse Fourier transform is used to obtain the time domain.

[58] **Acknowledgments.** This work is a contribution to the Greenland Ice Core Project (GRIP), a European Science Foundation program with eight nations (Belgium, Denmark, France, Germany, Iceland, Italy, Switzerland, and United Kingdom), and the EU, collaborating to drill through the central part of the Greenland ice sheet. Reviews by J. Kohler and C. Richardson-Näslund and recommendations by the Editors contributed to the final manuscript.

References

Ackley, S. F., and T. E. Keliher, Ice sheet internal radio-echo reflections and associated physical property changes with depth, *J. Geophys. Res.*, *84*, 5675–5680, 1979.

Alley, R. B., and B. R. Koci, Ice core analysis at Site A, Greenland: Preliminary results, *Ann. Glaciol.*, *10*, 1–4, 1988.

Bailey, J. T., S. Evans, and G. de Q. Robin, Radio echo sounding of polar ice sheets, *Nature*, *204*, 420–421, 1964.

Blindow, N., The central part of the Filchner-Ronne ice shelf Antarctica: Internal structures revealed by 40 MHz monopulse RES, *Ann. Glaciol.*, *20*, 365–371, 1994a.

Blindow, N., Reflection amplitudes of 40 MHz monopulse radio echo sounding: Correlation with ice core data and ice dynamics, in *Filchner Ronne Ice Shelf Programme, Report 8*, edited by H. Oerter, pp. 5–8, Alfred Wegener Inst. for Polar and Mar. Res., Bremerhaven, Germany, 1994b.

Bogorodsky, V. V., C. R. Bentley, and P. E. Gudmandsen, *Radioglaciology*, D. Reidel, Norwell, Mass., 1985.

Budden, K. G., *The Propagation of Radio Waves*, Cambridge Univ. Press, New York, 1985.

Camplin, G. C., and J. W. Glen, The dielectric properties of HF doped single crystals of ice, in *Physics and Chemistry of Ice*, edited by E. Whalley, S. J. Jones, and L. W. Gold, pp. 256–261, R. Soc. of Can., Ottawa, Ont., 1973.

Choate, W. C., A fast algorithm for normal incidence seismograms, *Geophysics*, *47*, 196–205, 1982.

Clough, J. W., Radio Echo sounding, reflections from internal layers in ice sheets, *J. Glaciol.*, *18*, 3–14, 1977.

Dansgaard, W., et al., Evidence for general instability of past climate from a 250-kyr ice-core record, *Nature*, *364*, 218–220, 1993.

Dennison, A. T., An introduction to synthetic seismogram techniques, *Geophys. Prospect.*, *8*, 231–241, 1960.

Evans, S., Progress report on radio echo sounding, *Polar Rec.*, *13*, 413–420, 1966.

Fujita, S., and S. Mae, Causes and nature of ice sheet radio-echo internal reflections estimated from the dielectric properties of ice, *Ann. Glaciol.*, *20*, 80–86, 1994.

Fujita, S., S. Mae, and T. Matsuoka, Dielectric anisotropy in ice Ih at 9.7 GHz, *Ann. Glaciol.*, *17*, 276–280, 1993.

Fujita, S., H. Maeno, S. Uratsuka, T. Furukawa, S. Mae, Y. Fujii, and O. Watanabe, Nature of radio echo layering in the Antarctic ice sheet detected by a two-frequency experiment, *J. Geophys. Res.*, *104*, 13,013–13,024, 1999.

Fujita, S., T. Matsuoka, T. Ishida, K. Matsuoka, and S. Mae, A summary of the complex dielectric permittivity of ice in the megahertz range and its application for radar sounding of polar ice sheets, in *Physics of Ice Core Records*, edited by T. Hondoh, pp. 185–212, Hokkaido Univ. Press, Sapporo, Japan, 2000.

Gerland, S., H. Oerter, J. Kipfstuhl, F. Wilhelms, H. Miller, and W. D. Miners, Density log of a 181 m long ice core from Berkner Island, Antarctica, *Ann. Glaciol.*, *29*, 215–219, 1999.

Glen, J. W., and J. G. Paren, The electric properties of snow and ice, *J. Glaciol.*, *15*, 15–38, 1975.

Goupillaud, P. L., An approach to inverse filtering of near-surface layer effects from seismic records, *Geophysics*, *26*, 754–760, 1961.

Gow, A. J., D. A. Meese, R. B. Alley, J. J. Fitzpatrick, S. Anandakrishnan, G. A. Woods, and B. C. Elder, Physical and structural properties of the Greenland Ice Sheet Project ice core: A review, *J. Geophys. Res.*, *102*, 26,559–26,575, 1997.

Gudmandsen, P., Layer echoes in polar ice sheets, *J. Glaciol.*, *15*, 95–101, 1975.

Gudmandsen, P., Studies of ice by means of radio echo sounding, *Rep. 162*, 22 pp., Electromagn. Inst., Tech. Univ. Denmark, Lyngby, 1976.

Hammer, C. U., Acidity of Polar ice cores in relation to absolute dating, past volcanism, and radio echos, *J. Glaciol.*, *25*, 359–372, 1980.

Hargreaves, N. D., The polarisation of radio signals in radio echo sounding of ice sheets, *J. Phys. D Appl. Phys.*, *10*, 1285–1304, 1977.

Hargreaves, N. D., The radio frequency birefringence of polar ice, *J. Glaciol.*, *21*, 301–313, 1978.

Harrison, C. H., Radio propagation effects in glaciers, Ph.D. thesis, Univ. of Cambridge, Cambridge, England, 1972.

Harrison, C. H., Radio echo sounding of horizontal layers in ice, *J. Glaciol.*, *12*, 383–397, 1973.

Hempel, L., and F. Thyssen, Deep radio echo soundings in the vicinity of GRIP and GISP2 drill sites, Greenland, *Polarforschung*, *62*, 11–16, 1992.

Hempel, L., F. Thyssen, N. Gundestrup, H. B. Clausen, and H. Miller, A comparison of radio echo sounding data and electrical conductivity of the GRIP ice core, *J. Glaciol.*, *46*, 369–374, 2000.

Hobbs, P. V., *Ice Physics*, Clarendon, Oxford, England, 1974.

Jacobel, R. W., and S. M. Hodge, Radar internal layers from the Greenland summit, *Geophys. Res. Lett.*, *22*, 587–590, 1995.

Jacobel, R. W., A. M. Glades, D. L. Gottschling, S. M. Hodge, and D. L. Wright, Interpretation of radar detected internal layer folding in West Antarctic ice streams, *J. Glaciol.*, *39*, 528–537, 1993.

Johnsen, S. J., N. S. Gundestrup, S. B. Hansen, J. Schwander, and H. Rufli, The new improved version of the ISTUK ice core drill, *Mem. Natl. Inst. Polar Res. Spec. Issue*, *49*, 9–23, 1994.

Johnsen, S. J., D. Dahl-Jensen, W. Dansgaard, and N. Gundestrup, Greenland palaeotemperatures derived from GRIP bore hole temperature and ice core isotope profiles, *Tellus, Ser. B*, *47*, 624–629, 1995.

Kovacs, A., A. J. Gow, and R. M. Morey, The in situ dielectric constant of polar firn revisited, *Cold Reg. Sci. Technol.*, *23*, 245–256, 1995.

Lanzario-Mancilla, O., and E. Gomez-Trevino, Synthetic radargrams from electrical conductivity and magnetic permeability variations, *J. Appl. Geophys.*, *34*, 283–290, 1996.

Matsuoka, T., S. Fujita, S. Morishima, and S. Mae, Precise measurement of dielectric anisotropy in ice Ih at 39 GHz, *J. Appl. Phys.*, *81*, 2344–2348, 1997a.

Matsuoka, T., S. Fujita, and S. Mae, Dielectric properties of ice containing ionic impurities at Microwave frequencies, *J. Phys. Chem. B*, *101*, 6219–6222, 1997b.

Millar, D. H. M., Radio-echo layering in polar ice sheets, Ph.D. thesis, Univ. of Cambridge, Cambridge, England, 1981a.

Millar, D. H. M., Radio-echo layering in polar ice sheets and past volcanic activity, *Nature*, *292*, 441–443, 1981b.

Millar, D. H. M., Acidity levels in ice sheets from radio echo-sounding, *Ann. Glaciol.*, *3*, 199–203, 1982.

Miners, W. D., Electromagnetic reflections inside ice sheets, Ph.D. thesis, Open Univ., Milton Keynes, England, 1998.

Miners, W. D., and R. Mulvaney, Electrical logging and initial dating of the ice cores from Berkner 94/95, in *Filchner Ronne Ice Shelf Programme, Report 9*, edited by H. Oerter, pp. 64–66, Alfred Wegener Inst. for Polar and Mar. Res., Bremerhaven, Germany, 1995.

Miners, W. D., A. Hildebrand, S. Gerland, N. Blindow, D. Steinhage, and E. W. Wolff, Forward modelling of the internal layers in radio echo sounding using electrical and density measurements from ice cores, *J. Phys. Chem. B*, *101*, 6201–6204, 1997.

Moore, J. C., Geophysical aspects of ice core drilling in Antarctica, Ph.D. thesis, Counc. of Natl. Acad. Awards, Br. Antarct. Surv., Cambridge, England, 1988a.

Moore, J. C., Dielectric variability of a 130 m Antarctic ice core: Implications for radar sounding, *Ann. Glaciol.*, *11*, 95–99, 1988b.
Moore, J. C., and J. G. Paren, A new technique for dielectric logging of Antarctic ice cores, *J. Phys.*, *48*, C1/155–C1/160, 1987.
Moore, J. C., J. G. Paren, and H. Oerter, Sea salt dependent electrical conduction in polar ice, *J. Geophys. Res.*, *97*, 19,803–19,812, 1992a.
Moore, J. C., E. W. Wolff, H. B. Clausen, and C. U. Hammer, The chemical basis for the electrical stratigraphy of ice, *J. Geophys. Res.*, *97*, 1887–1896, 1992b.
Moore, J. C., E. W. Wolff, H. B. Clausen, C. U. Hammer, M. R. Legrand, and K. Fuher, Electrical response of the Summit-Greenland ice core to ammonium, sulphuric acid and hydrochloric acid, *Geophys. Res. Lett.*, *21*, 565–568, 1994.
Nielsen, P. H., Calculation of synthetic reflection seismograms in the frequency domain, *Geophys. Prospect.*, *26*, 399–406, 1978.
Nishio, F., and H. Ohmae, Internal radio-echo reflections of polar snow covers in relation to acidic layers and density fluctuations, *Ann. Glaciol.*, *6*, 289–291, 1985.
O'Doherty, R. F., and N. A. Anstey, Reflections on amplitudes, *Geophys. Prospect.*, *19*, 430–458, 1971.
Paren, J. G., Dielectric properties of ice, Ph.D. thesis, Univ. of Cambridge, Cambridge, England, 1970.
Paren, J. G., Reflection coefficient at a dielectric interface, *J. Glaciol.*, *27*, 203–204, 1981.
Paren, J. G., and G. de Q. Robin, Internal reflections in polar ice sheets, *J. Glaciol.*, *14*, 251–259, 1975.
Paterson, W. S. B., *The Physics of Glaciers*, 3rd ed., 480 pp., Elsevier Sci., New York, 1994.
Peterson, R. A., W. R. Fillippone, and F. B. Coker, The synthesis of seismograms from well log data, *Geophysics*, *20*, 516–538, 1955.
Petrenko, V. F., Electrical properties of ice, *CRREL Spec. Rep. 93-20*, Cold Reg. Res. and Eng. Lab., Hanover, N. H., 1993.
Rees, W. G., and R. E. Donovan, Refraction correction for radio echo sounding of large ice masses, *J. Glaciol.*, *38*, 302–308, 1992.
Robin, G. de Q., S. Evans, and J. T. Bailey, Interpretation of Radio echo sounding in Polar Ice sheets, *Philos. Trans. R. Soc. London, Ser. A*, *265*, 437–505, 1969.
Sihvola, A. H., and I. V. Lindell, Polarizability modelling of heterogeneous media, in *Dielectric Properties of Heterogeneous Materials, Progress in Electromagnetics Research Book 6 (PIERS 6)*, edited by A. Priou, pp. 101–151, EMW, Cambridge, Mass., 1992.
Sihvola, A. H., E. Nyfors, and M. Tiuri, Mixing formulae and experimental results for the dielectric constant of snow, *J. Glaciol.*, *31*, 163–170, 1985.
Skou, N., and F. Sondergaard, Radioglaciology A 60 MHz ice sounder system, *Rep. R169*, 124 pp., Electromagn. Inst., Tech. Univ. Denmark, Lyngby, 1976.
Staelin, D. H., A. W. Morgenthaler, and J. A. Kong, *Electromagnetic Waves*, Prentice-Hall, Old Tappan, N. J., 1994.
Stiles, W. H., and F. T. Ulaby, Dielectric properties of snow, *CRREL Spec. Rep. 82-18*, Cold Reg. Res. and Eng. Lab., Hanover, N. H., 1981.
Stock, J., Vorwärtsmodellierung von EMR-Spuren mit Bohrkerndaten vom Filchner-Ronne-Schelfeis, Antarktis, Diplomarbeit im fach Geophysik, Inst. für Geophys., Westfalische Wilhelms-Univ., Münster, Germany, 1993.
Thorsteinsson, T., J. Kipfstuhl, and H. Miller, Textures and fabrics in the GRIP ice core, *J. Geophys. Res.*, *102*, 26,583–26,599, 1997.
Trorey, A. W., Theoretical seismograms with frequency and depth dependent absorption, *Geophysics*, *27*, 766–785, 1962.
Wait, J. R., Transmission and reflection of electromagnetic waves in the presence of stratified media, *J. Res. Natl. Bur. Stand.*, *61*, 205–232, 1958.
Wait, J. R., *Electromagnetic Waves in Stratified Media*, Oxford Univ. Press, New York, 1996.
Whillans, I. M., Radio echo layers and the recent stability of the West Antarctic ice sheet, *Nature*, *264*, 152–155, 1976.
Wolff, E. W., Electrical stratigraphy of polar ice cores: Principle, methods and findings, in *Physics of Ice Core Records*, edited by T. Hondoh, pp. 155–171, Hokkaido Univ. Press, Sapporo, Japan, 2000.
Wolff, E. W., J. C. Moore, H. B. Clausen, C. U. Hammer, J. Kipfstuhl, and K. Fuhrer, Long term changes in the acid and salt concentrations of the Greenland Ice Core Project ice core from electrical stratigraphy, *J. Geophys. Res.*, *100*, 16,249–16,263, 1995.
Wright, D. L., J. A. Bradley, and S. M. Hodge, Use of a New High speed Digital Data Acquisition System in Airborne Ice Sounding, *IEEE Trans. Geosci. Remote Sens.*, *27*, 561–567, 1989.
Yoshida, M., K. Yamashita, and S. Mae, Bottom topography and internal layers in East Dronning Maud Land, East Antarctica, from 179 MHz radio echo-sounding, *Ann. Glaciol.*, *9*, 221–224, 1987.

L. Hempel, Rathausstrasse 13, D-58239 Schwerte, Germany. (Ludwig.Hempel@t-online.de)
R. Jacobel, Department of Physics, St. Olaf College, 1500 St. Olaf Ave, Northfield, MN 55057, USA. (jacobel@stolaf.edu)
W. D. Miners, 23 Orchard Way, Harwell, Didcot, Oxfordshire OX11 0LQ, UK. (William.Miners@btinternet.com)
J. C. Moore, Arctic Centre, University of Lapland Box 122, FIN-96101, Rovaniemi, Finland. (john.moore@urova.fi)
E. W. Wolff, British Antarctic Survey, High Cross, Madingley Road, Cambridge, CB3 0ET, UK. (e.wolff@bas.ac.uk)